Journal of Cluster Science (2024) 35:1889–1902
https://doi.org/10.1007/s10876-024-02632-x

ORIGINAL PAPER

Investigating the Antibacterial Effectiveness of Zinc Particles in Different Forms within Alginate-Based Hydrogels Incorporating Nanocellulose

Muhamad Alif Razi[1,2] · Gerald Ensang Timuda[3] · Deni Shidqi Khaerudini[3] · Ni Putu Ratna Ayu Krishanti[4] · Andri Pramesyanti Pramono[5] · Luciasih Agustini[6] · Wahyu Ramadhan[7,9] · Safrina Dyah Hardiningtyas[7] · Maya Ismayati[2] · Novitri Hastuti[2,8]

Received: 8 March 2024 / Accepted: 29 April 2024 / Published online: 9 May 2024

Abstract

In contrast to zinc oxide (ZnO), the antibacterial potential of zinc hydroxyacetate (Zn-HA) remains unexplored. In this study, we fabricated alginate/TEMPO-oxidized nanocellulose (AT) hydrogels containing three types of zinc particles (Zn Ps): Zn-HA, Zn-N (ZnO nanoparticles), and Zn-C (commercial ZnO). The antibacterial efficacy of these hydrogels was assessed and compared. The integration of Zn Ps into AT hydrogels was achieved through a facile method, resulting in the formation of composite hydrogels with layered three-dimensional structures. The addition of Zn Ps reduced the mechanical properties and swelling ability of the hydrogels. The antibacterial activities of the Zn Ps and hydrogels were evaluated using the disc diffusion method. Surprisingly, Zn-HA exhibited significantly stronger antibacterial efficacy against both *E. coli* and *S. aureus*, with the zone of inhibition (ZOI) ranging from 11 mm to 19.7 mm compared to Zn-C and Zn-N (ZOI of 8.3–9.3 mm). This improved antibacterial activity might be attributed to the higher release of Zn^{2+} from Zn-HA (7.5 mg/100 mL compared to 0.8 and 1.2 mg/100 mL), as evidenced by the zinc dissolution study. The antibacterial activity of the AT hydrogels was significantly enhanced by the inclusion of Zn-HA but not Zn-C or Zn-N. All hydrogels exhibited mild toxicity to human skin fibroblasts. In summary, our findings challenge the expectation that ZnO (Zn-C and Zn-N) would have better antibacterial properties due to their smaller particle sizes in comparison to Zn-HA microparticles. Additionally, our results indicate that converting Zn-HA to ZnO is unnecessary to impart antibacterial properties to the hydrogels. Thus, AT hydrogels containing Zn-HA (ATZ-HA) can potentially be used as advanced antibacterial materials, possibly for use in wound dressings.

✉ Muhamad Alif Razi
alifrazi@upnvj.ac.id

[1] Faculty of Engineering, Universitas Pembangunan Nasional Veteran Jakarta, Depok 12450, Indonesia

[2] Research Center for Biomass and Bioproducts, National Research and Innovation Agency (BRIN), Kawasan Sains Teknologi Dr. (H.C.) Ir. H. Soekarno Jl. Raya Bogor Km. 46, Cibinong 16911, Indonesia

[3] Research Center for Advanced Materials, National Research and Innovation Agency (BRIN), South Tangerang 15314, Indonesia

[4] Research Center for Applied Zoology, National Research and Innovation Agency (BRIN), Kawasan Sains Teknologi Dr. (H.C.) Ir. H. Soekarno Jl. Raya Bogor Km. 46, Cibinong 16911, Indonesia

[5] Research Center for Molecular Biology Eijkman, National Research and Innovation Agency (BRIN), Kawasan Sains Teknologi Dr. (H.C.) Ir. H. Soekarno Jl. Raya Bogor Km. 46, Cibinong 16911, Indonesia

[6] Research Center for Applied Microbiology, National Research and Innovation Agency (BRIN), Kawasan Sains Teknologi Dr. (H.C.) Ir. H. Soekarno Jl. Raya Bogor Km. 46, Cibinong 16911, Indonesia

[7] Department of Aquatic Product Technology, Faculty of Fisheries and Marine, IPB University, Bogor 16680, Indonesia

[8] Research Collaboration Center for Nanocellulose, Andalas University-BRIN, Padang, Sumatera Barat, Indonesia

[9] Center for Coastal and Marine Resources Studies (PKSPL), Bogor, West Java 16127, Indonesia

Highlights

- Synthesis of alginate/TOCN (AT) hydrogels incorporating different forms of zinc particles, i.e., zinc hydroxyacetate (Zn-HA), commercial ZnO (Zn-C), and ZnO nanoparticles (Zn-N).
- Zn-HA displayed significantly stronger antibacterial efficacy against *E. coli* and *S. aureus* compared to Zn-C and Zn-N.
- Zn-HA enhanced the antibacterial efficiency of AT hydrogels, but it reduced their mechanical, crystallinity, and swelling properties.
- AT hydrogels containing Zn-HA (ATZ-HA) hold the potential as advanced antibacterial materials, possibly for wound dressings.

Graphical Abstract

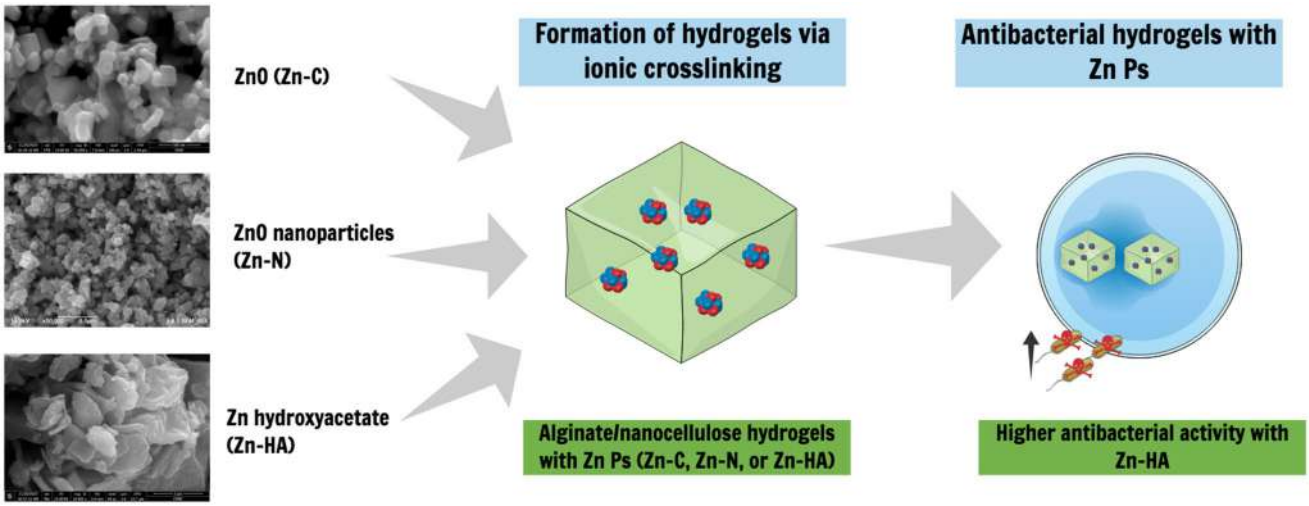

Keywords Alginate · Nanocellulose · Zinc hydroxyacetate · ZnO · Antibacterial activity

Introduction

The use of environmentally friendly organic materials such as polysaccharides for the research and development of composite materials has become a popular trend in recent years. Polysaccharides, derived from renewable sources such as plants and algae, offer numerous advantages over traditional synthetic materials because they are abundant, biodegradable, and non-toxic, making them ideal for various applications in industries such as food and health sectors [1, 2].

Alginate and nanocellulose are potentially attractive polysaccharides that can be used as composite materials. Alginate is a naturally occurring polysaccharide derived from brown seaweed that consists of β-D-mannuronic acid (M) and α-L-guluronic acid (G) [3, 4]. Nanocellulose, on the other hand, is a nanoscale cellulose material with unique mechanical properties and a high surface area [5]. Both are considered promising materials for various applications owing to their abundance, biodegradability, and sustainability [6].

Composite materials comprising alginate and nanocellulose show promise for various applications such as bioprinting, biomedical, and tissue engineering [7–10]. For instance, the unique combination of nanocellulose shear-thinning properties and the viscous nature of alginate allows the formation of hydrogels with divalent cations under physiological conditions, making them highly appealing for bioprinting purposes [7]. In addition, nanocellulose can improve the structural, mechanical, and chemical stability of alginate hydrogels, as indicated by the occurrence of 3D fibrous structures, reduction of alginate syneresis, and increase in resistance and Young's modulus, which allows biomedical application of these composite hydrogels for the encapsulation of cells and tissue engineering [8–10].

Although composite alginate/nanocellulose hydrogels have shown promising chemical and physical properties, their functionalities, such as antibacterial activity, are often limited to more advanced biomedical applications, such as wound dressings [11]. To overcome this limitation, researchers have explored new strategies such as incorporating antimicrobial agents into the composite hydrogel matrix. This approach aims to enhance the antibacterial

activity of composite alginate and nanocellulose hydrogels, making them more effective in combating bacterial infections. Zinc oxide (ZnO) is one of the most widely used antimicrobial agents and has been shown to be suitable for use as a bioactive wound dressing material [12, 13]. The antibacterial ability of ZnO is postulated to be due to the release of Zn^{2+} ions into membrane cells, production of reactive oxygen species (ROS), and disruption and penetration of bacterial membrane cells, which trigger DNA denaturation, mitochondrial dysfunction, protein oxidation, and leakage of intracellular components [14–17]. Moreover, ZnO has been reported to promote fibroblast proliferation, which enhances re-epithelialization [18]. These properties hold promise for the development of biofunctionalized materials for various applications such as advanced wound dressings or food packaging.

Previous studies have predominantly focused on composite hydrogels incorporating ZnO nanoparticles (ZnO NPs), which exhibit enhanced properties and antibacterial activity [19–21]. For example, Varaprasad et al. fabricated sodium alginate-coated cellulose fibers impregnated with ZnO NPs using a simple precipitation technique, which showed enhanced thermal stability, mechanical properties, and excellent antibacterial activity [22]. Shefa et al. successfully designed 2,2,6,6-tetramethylpiperidine-1-oxyl radical (TEMPO)-oxidized cellulose nanofiber (TOCN)/polyethylene glycol/ZnO hydrogels with tailored mechanical properties and remarkable hemostatic activity that decreased bleeding time [23]. However, there is a clear research gap in the exploration of the potential benefits of utilizing zinc hydroxyacetate (Zn-HA), an intermediate compound formed prior to the conversion of ZnO through heat treatment, in terms of its usefulness as a functional antibacterial material. Thus, a comparative study between ZnO and Zn-HA warrants investigation, as this could provide insights into the role of different zinc particles (Zn Ps) in killing bacteria. The aim of this study was to assess and compare the antibacterial efficacy of different forms of Zn Ps and to evaluate the effect of Zn Ps on the physical and antibacterial properties of composite alginate/nanocellulose hydrogels. In this study, three zinc particles (Zn Ps), i.e., commercially available ZnO (Zn-C), ZnO nanoparticles (Zn-N), and zinc hydroxyacetate (Zn-HA) were used and compared. The physical characteristics of the hydrogels, such as their swelling behavior, were analyzed to determine the effect of embedded Zn Ps. Finally, the antibacterial activity of the composite hydrogels containing Zn Ps was tested against a range of bacterial strains to assess their potential as antibacterial materials. The novelty of this study is highlighted by two main aspects. Firstly, it shows the first comparative study on the antibacterial efficacy of different Zn Ps. Secondly, it highlights the potential use of Zn-HA as an effective antibacterial material in composite alginate/nanocellulose hydrogels. This research contributes to the understanding of the role of Zn Ps in enhancing the antibacterial properties of composite hydrogel materials, providing valuable insights that could lead to the development of functional composite hydrogels suitable for biomedical or pharmaceutical applications.

Materials and Methods

Materials

Zinc acetate dihydrate, sodium hydroxide (NaOH), ethanol, and calcium chloride ($CaCl_2$) were purchased from Merck (Jakarta, Indonesia). Sodium alginate was obtained from Sigma-Aldrich Co. Ltd. (Jakarta, Indonesia). Commercial ZnO (Zn-C) was purchased from Loba Chemie Pvt., Ltd. (Mumbai, India). TEMPO (2,2,6,6-tetramethylpiperidine 1-oxyl)-oxidized cellulose nanofibers (TOCN) were used as previously described in our previous research [24]. All chemicals were of analytical grade and were used without further purification.

Synthesis and Characterization of Zn Ps Via the Precipitation Method

Zn Ps were synthesized via the precipitation method [25–27] where zinc acetate dihydrate was used as a precursor and dissolved in ethanol at a concentration of 0.1 M. 1 M NaOH was added dropwise into the zinc ethanolic solution under agitated magnetic stirring (300 rpm) at room temperature (25 ^{o}C) until white solutions were formed. The reaction was continued for 2 h. Then, centrifugation at 8000 rpm for 15 min was performed to collect the white solid precipitate, followed by washing twice with distilled water and ethanol. The white solid precipitate was dried in an oven at 80 ^{o}C for 24 h to produce zinc hydroxyacetate (Zn-HA). Some parts of the white solid precipitates were taken and calcined in a tube furnace at 600 ^{o}C for 2 h at a heating rate of 5 ^{o}C /min to produce ZnO nanoparticles (Zn-N).

The characterization of the synthesized Zn particles (Zn Ps) was done using X-ray diffraction (XRD) and Field Emission Scanning Electron Microscopy (FE SEM) coupled with energy-dispersive X-ray spectroscopy (EDX) analysis. Powder samples were used for characterization. The crystalline patterns were analyzed on an XRD Instrument at intervals of 5^{o}–80^{o} (2θ range). The size and morphology of the synthesized Zn Ps were determined using a JEOL FE SEM (JIB 4610 F) or FEI Quanta 650 at an accelerating voltage of 15 or 25 kV with a gold coating to avoid the charging effect.

Fabrication and Characterization of Alginate/TOCN/Zn Ps Hydrogels

Hydrogels comprising alginate, TOCN, and Zn Ps were fabricated via ionic cross-linking using $CaCl_2$. In a typical procedure, sodium alginate powder was dissolved in distilled water at a concentration of 3wt% using a magnetic stirrer. Zn Ps (Zn-N, Zn-C, and Zn-HA) at a concentration of 20 mg/mL were added to the alginate solution (3 mL) and sonicated for 30 min in an ultrasonic water bath. TOCN dissolved in distilled water (1wt%) was then added to the alginate/Zn solution at a volume ratio of 1:1 (3 mL) and mixed homogenously using a vortex mixer. The solutions were cast on a petri dish and immersed in $CaCl_2$ solution (3%) for 1 h. The resulting hydrogels were carefully peeled from the petri dishes and characterized.

The cross-sectional images of the hydrogels were analyzed using SEM. The hydrogels were then freeze-dried for 24 h. The lyophilized samples were sliced and coated with gold before SEM analysis (Hitachi SU3500) at an acceleration voltage of 10 kV. EDX analysis was also performed to confirm the presence of Zn Ps in the hydrogels. Fourier-transform infra-red (FTIR) spectroscopy analysis was also performed on the hydrogel films. The mechanical strength of the hydrogels was determined using a universal testing machine with a load cell of 10kN in the dry state. Both ends of the hydrogel films with dimensions of 6 cm x 1 cm were clipped. The swelling of the hydrogels was determined by immersing freeze-dried hydrogels in distilled water at 37 ^{o}C and pH 7. At predetermined times, swollen hydrogels were taken, and the water not taken up by the hydrogels was removed using tissue paper and weighed. Then, the hydrogels were immersed again in distilled water. This step was repeated for 24 h. The swelling (%) was calculated using the following equation [28]:

$$\text{Swelling } (\%) = \left(\frac{\mathrm{W_s} - \mathrm{W_i}}{\mathrm{W_i}}\right) \times 100$$

Where, W_i and W_s are the weights of freeze-dried hydrogels in the initial and swollen states, respectively.

Antibacterial Activities of the Zn Ps and Hydrogels

The antibacterial activities of the hydrogels were evaluated by the disc diffusion method [29] against *S. aureus* and *E. coli*, as representatives of gram-positive and gram-negative bacteria, respectively. The hydrogels were cut into spherical shapes and sterilized using ethanol. The hydrogels were then deposited on an agar plate containing bacteria prior to incubation for 24 h at 37^{o}C. The diameter of the inhibition zone was measured to assess the antibacterial activity of the hydrogels. In addition, the percentage inhibition (%) was determined by dividing the diameter of the inhibition zone (total diameter) by the diameter of the hydrogels multiplied by 100. The antibacterial activities of the Zn Ps were also evaluated using the disc diffusion method. The 8-mm diameter sample discs containing Zn Ps dissolved in DMSO at varying concentrations (5, 10, and 20 mg/mL) were placed on an agar plate. Similarly, the diameter of the inhibition zone and percentage inhibition (%) were measured to assess the antibacterial activity of the Zn Ps. The experiments were conducted in triplicate.

In Vitro Biocompatibility of Hydrogels

The in vitro biocompatibility of the hydrogels was evaluated using human skin fibroblasts isolated from the preputium. The study protocol was approved by the Ethics Committee of the Faculty of Medicine, Universitas Pembangunan Nasional Veteran Jakarta, Indonesia, No. 7/I/2024/KEP. The cells were cultured in Dulbecco's Modified Eagle's medium (DMEM) with low glucose (Gibco, USA) supplemented with 10% fetal bovine serum (FBS) (Gibco, USA) and 1% penicillin-streptomycin. Cells were incubated in a humidified atmosphere containing 5% CO_2 at 37^{o}C for 24 h. The 3-(4,5-dimethylthiazol-2-yl)-5-(3-carboxymethoxyphenyl)-2-(4-sulfophenyl)-2 H-tetrazolium (MTS) assay was utilized to determine the in vitro biocompatibility and cell viability of the hydrogels according to a previously described method [30] with slight modifications. Briefly, the hydrogels were sterilized by UV treatment for 4 h. Subsequently, the samples were subjected to incubation with low glucose DMEM without FBS for 24 h to obtain hydrogel extracts at a concentration of 0.1 mg/mL. Simultaneously, the cells were seeded in a 96-well plate at a concentration of $5x10^3$ cells/well and incubated for 24 h. The medium was then replaced with the hydrogel extracts and incubated for 24 h. MTS reagent was then added to each well and the plate was incubated at 37^{o}C for 24 h. The absorbance was measured directly using a microplate reader at a wavelength of 490 nm. The cell viability was determined by dividing the absorption of each sample by that of the control (without sample). The experiments were performed in triplicate.

Results and Discussion

Synthesis and Characterization of Zn Ps

Three types of Zn Ps (Zn-N, Zn-HA, and Zn-C) were used and compared in this study. Zn-N and Zn-HA were synthesized via a precipitation method in an ethanolic solution, whereas Zn-C was commercially obtained. In the case of

Zn-N, calcination was performed, but this was not applied to Zn-HA. Figure 1a shows the FE-SEM photographs of the Zn Ps. Zn-N was spherical and showed a quite uniform size distribution (Fig. 1b). The measured particle sizes were in the range of 100 nm (101 ± 40 nm). On the other hand, Zn-C showed a more heterogeneous morphology, displaying rod-like and quasi-spherical shapes. Its particle size (213 ± 69 nm) was larger than that of Zn-N. Interestingly, Zn-HA exhibited plate-like structures with sizes ranging from one to several micrometers (3.9 ± 1.8 µm). Zeta potential analysis showed that all three Zn Ps had negative surface charges, with the highest value observed for Zn-N (-34.7 mV) and the lowest for Zn-HA (-16.7 mV) (Fig. S1). These values indicate a satisfactory colloidal stability. Figure 1c shows the XRD patterns of Zn Ps. The XRD pattern of Zn-N closely resembles that of Zn-C. The diffraction peaks observed at 2θ angles of 32°, 34.4°, 36.3°, 47.5°, 56.6°, 62.8°, 66.4°, 67.9°, and 69° provide evidence that Zn-N and Zn-C were ZnO with a wurtzite structure [31]. In contrast, the XRD spectra of Zn-HA did not show the characteristic peaks of ZnO [27], as expected. These findings align with prior research, which indicates that the process of high-temperature calcination is crucial for converting Zn-HA into ZnO with a highly crystalline wurtzite structure [32].

Energy dispersive X-ray (EDX) analysis was performed on the Zn Ps. EDX is a method that analyzes the elemental composition of a material by detecting the X-rays emitted when the nucleus of an atom in the material is struck by the primary beam of electrons [33]. EDX analysis and elemental mapping confirmed the presence of zinc (Zn) and oxygen (O) in Zn Ps with few impurities, indicating good purity (Fig. 2a-c). Figure 2d shows the atomic weight percentages (At%) of Zn-C, Zn-N, and Zn-HA. All Zn Ps showed a high percentage of Zn, accounting for more than 50% of the overall elemental composition. Notably, Zn-HA displayed a higher percentage of Zn at 60%, compared to Zn-C and Zn-N. The compositions of Zn and O in Zn-HA and Zn-C were similar. On the other hand, Zn-N contained 48% Zn and 52% O. These findings indicate that the elemental composition of Zn-N closely matches the theoretical atomic composition of ZnO [32].

Fabrication and Characterization of Alginate/TOCN/Zn Ps Hydrogels

The formation of alginate/TOCN (AT) hydrogels involves ionic crosslinking of alginate using $CaCl_2$ with fibrillar TOCN (Fig. S2) as a reinforcing filler. This crosslinking process creates a three-dimensional network structure that

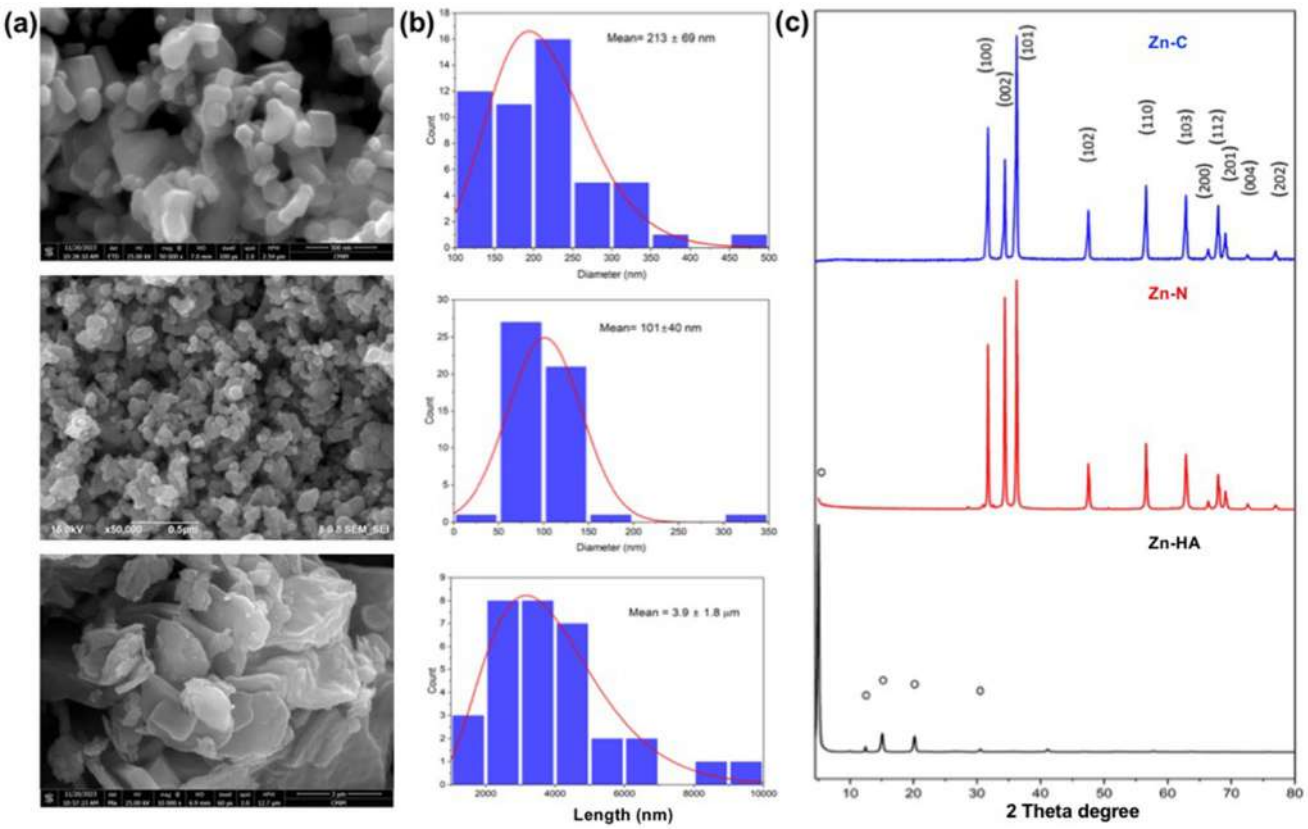

Fig. 1 Representative FE SEM images of Zn Ps (Zn-C, Zn-N, and Zn-HA) (**a**), Particle size distribution (**b**), and XRD patterns of Zn Ps (**c**)

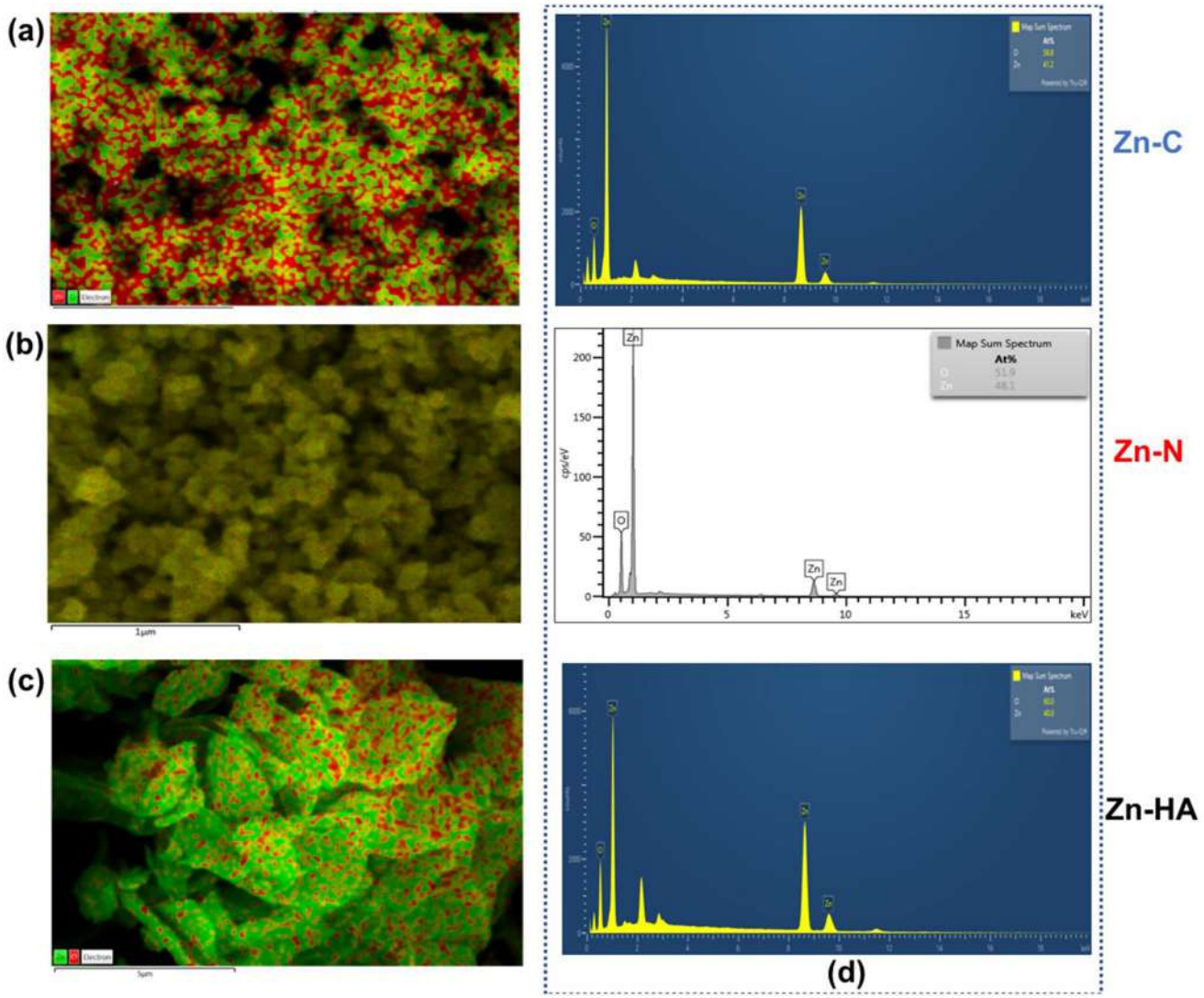

Fig. 2 The elemental mapping images of Zn Ps (Zn-C, Zn-N, and Zn-HA) (**a**-**c**) and the EDX analysis of Zn Ps (**d**)

provides a hydrogel with good mechanical strength and stability [11]. The incorporation of TOCN might enhance the properties of hydrogels such as their water retention capacity, mechanical properties, and biocompatibility [8, 9]. Zn Ps (Zn-N, Zn-HA, and Zn-C) were incorporated into the AT hydrogels by a simple addition and mixing process, which allows the facile production of composite ATZ-N, ATZ-HA, and ATZ-C hydrogels, respectively. Photographs of the hydrogels are shown in Fig. 3a. The cross-sectional morphologies of the composite hydrogels were evaluated using SEM (Fig. 3b). Layered and interconnected 3D structures were observed in all hydrogels, which indicates that the effect of Zn Ps on the morphology of the AT hydrogels was minimal. EDX analysis confirmed the existence of $CaCl_2$, which contributed to the formation of the 3D interpenetrating network hydrogels, and the Zn Ps were distributed in the hydrogel matrix (Fig. 3c and Fig. S3). FT-IR analysis was conducted to evaluate the chemical interactions between the Zn Ps and AT hydrogels. Figure 4 shows the FT-IR spectra of alginate, TOCN, and hydrogels with and without Zn Ps. The FT-IR spectra of the AT hydrogels are characterized by absorption bands at 3340 cm^{-1}, 2921 cm^{-1}, 1597 cm^{-1}, 1423 cm^{-1}, and 1024 cm^{-1} corresponding to the stretching vibration of the OH groups of alginate and TOCN, the stretching vibration of the −CH group in cellulose, the stretching vibration of carboxyl groups, the C = O bending vibrations of carbonyl groups, and the C–O stretching vibrations of cellulose, respectively [1, 8, 34, 35]. The stretching vibration of Zn–O bonds at around 400–500 cm^{-1} was not clearly detected in the ATZ-N, ATZ-HA, and ATZ-C hydrogels, possibly because of the dominance of the alginate/TOCN signals. However, the addition of Zn Ps tended to decrease the % transmittance of AT hydrogels at absorption bands at 3340 cm^{-1}, 1597 cm^{-1}, and 1423 cm^{-1}, suggesting

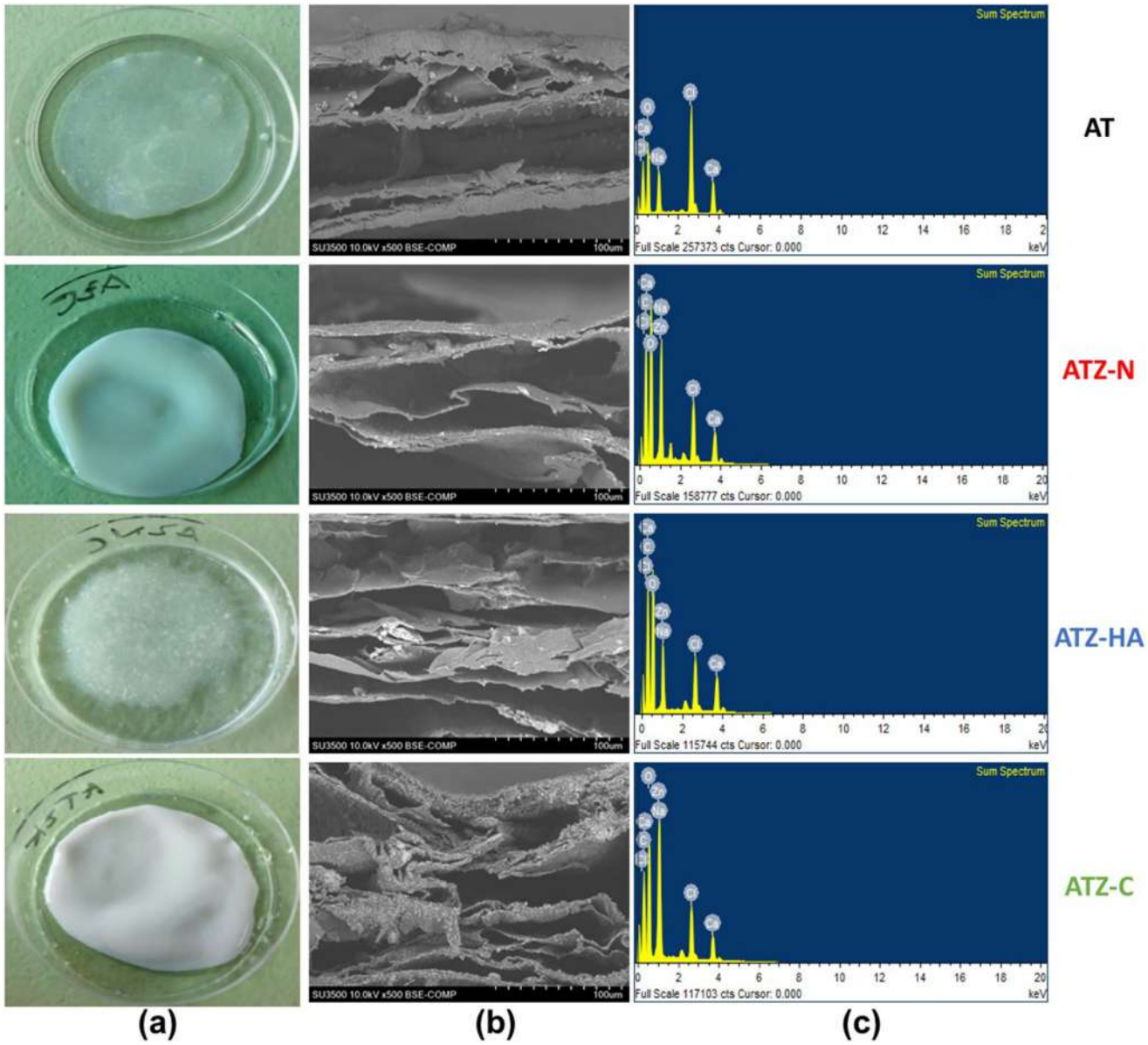

Fig. 3 Photographs of the hydrogels (**a**), cross-sectional morphology (**b**), and elemental composition of the hydrogels as determined by SEM-EDX analysis (**c**)

the presence of Zn Ps in AT hydrogels and possible interaction between them.

The crystallographic structures of alginate, TOCN, and the hydrogels were evaluated by XRD analysis (Fig. 5a and Fig.S4). The XRD patterns revealed that the AT hydrogels had a highly crystalline structure, which was attributed to the presence of calcium crosslinking and TOCN, and the presence of Zn Ps in the hydrogels was clearly detected. However, the addition of Zn Ps into AT hydrogels considerably decreased their crystallinity, as evidenced by the decrease in the XRD peaks at 22°, 29° and 31° associated with the AT hydrogel crystalline structure, particularly for ATZ-HA (Fig. 5b).

Swelling is an important property of hydrogels, as it enables them to absorb large amounts of water or other liquids [36]. Swelling in a hydrogel material is the expansion of the space between the polymer chains due to the penetration of water molecules into the polymer network [37, 38]. The swelling behavior of the hydrogels over a period of 24 h is presented in Fig. 6a. The AT hydrogels exhibited the highest swelling, reaching approximately 1300% within 4 h and maintaining a stable swollen state thereafter. The addition of Zn Ps into the AT hydrogels considerably decreased swelling, as evidenced by the decrease in the swelling percentage of ATZ-N, ATZ-C, and ATZ-HA at 1000, 660, and 470%, respectively, after 24 h. This decrease is attributed to the

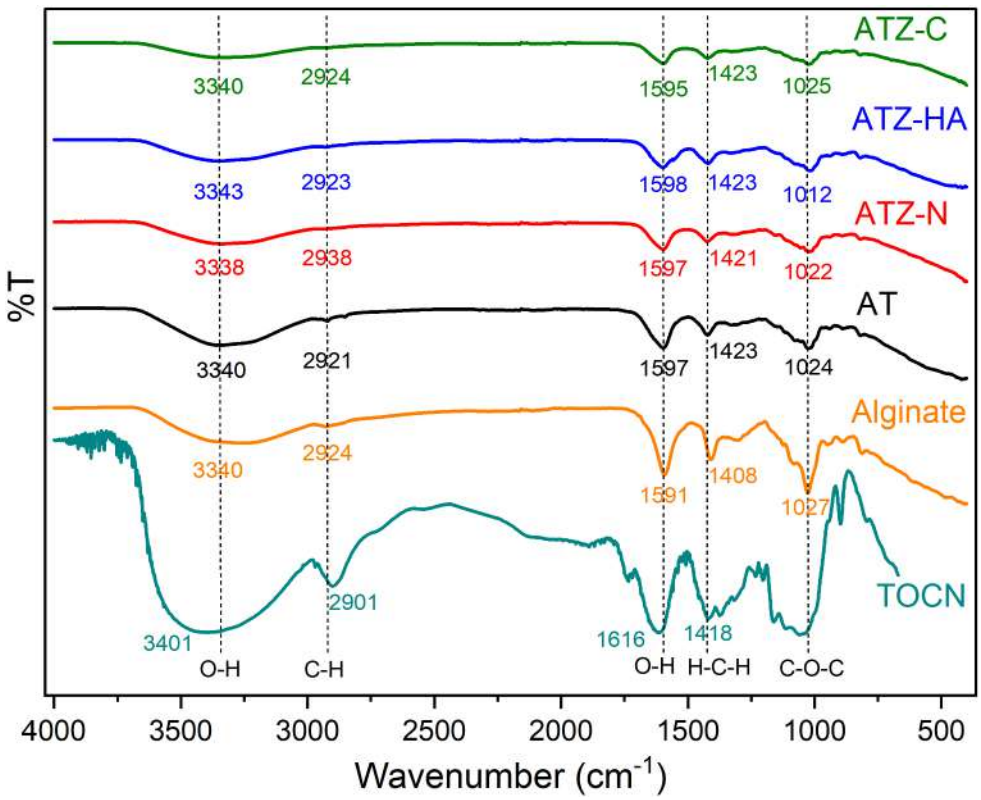

Fig. 4 ATR-FTIR spectra of TOCN, alginate, alginate/TOCN hydrogels (AT), and AT/Zn Ps hydrogels (ATZ-N, ATZ-HA, and ATZ-C)

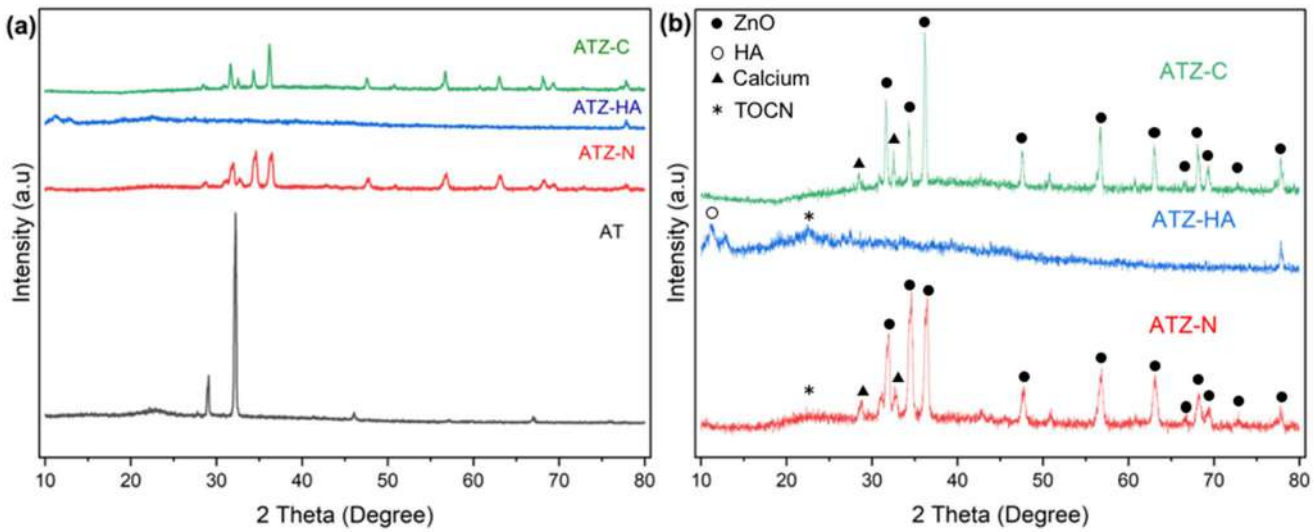

Fig. 5 XRD patterns of alginate/TOCN hydrogels (AT) and alginate/TOCN/Zn Ps hydrogels (**a**) and an enlarged image of the XRD patterns of alginate/TOCN/Zn Ps hydrogels (**b**)

restricted movement of polymer chains associated with the presence of Zn Ps, which reduces water absorption and prevents water molecules from interacting with free hydroxyl groups to form hydrogen bonds with the polymer matrix [38–40]. ATZ-HA showed the lowest swelling of approximately 470%, which might be due to stronger hydrogen bond interactions with the polymer chains that prevent water absorption. The tensile strength of the hydrogels was measured to evaluate their mechanical strength. Figure 6b shows the stress-strain curves of the composite hydrogels. AT hydrogels exhibited the highest tensile strength (13.3 N/mm^2) compared to those containing Zn Ps (less than 9.8 N/mm^2), indicating that the addition of ZnO or Zn-HA reduces the mechanical properties of AT hydrogels. These results agree with those of a previous study that used nanocomposite films based on hydroxypropyl methylcellulose/

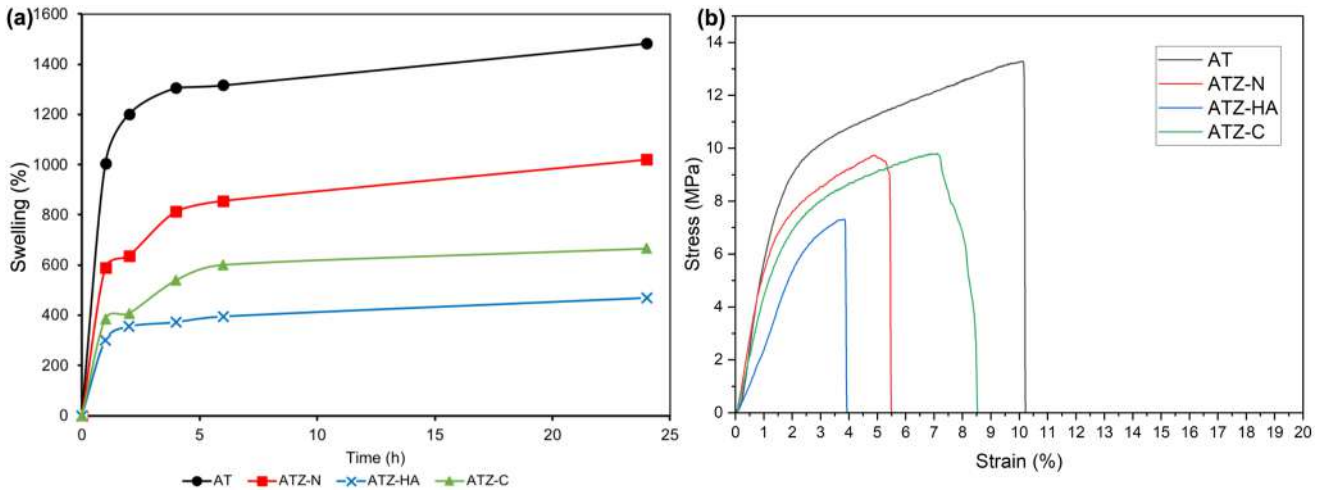

Fig. 6 The swelling of the hydrogels at distilled water pH 7 (**a**), and tensile stress-strain curves of the hydrogels

Table 1 The results of zone of inhibition (ZOI) and inhibition percentage for Zn Ps at varying concentrations (5,10, and 20 mg/mL)

No	Samples	Type of bacteria			
		E. coli		S. aureus	
		Zone of inhibition (ZOI)			
		Diameter (mm)	% Inhibition	Diameter (mm)	% Inhibition
1	5 mg/mL Zn-HA	11.3 ± 0.6	42	11.0 ± 1.7	38
2	5 mg/mL Zn-N	8.0 ± 0	0	8.0 ± 0	0
3	5 mg/mL Zn-C	8.7 ± 0.6	8	8.0 ± 0	0
4	10 mg/mL Zn-HA	13.0 ± 1.0	63	16.3 ± 1.2	104
5	10 mg/mL Zn-N	8.3 ± 0.6	4	8.0 ± 0	0
6	10 mg/mL Zn-C	9.0 ± 0	13	8.0 ± 0	0
7	20 mg/mL Zn-HA	16.0 ± 1	100	19.7 ± 0.6	146
8	20 mg/mL Zn-N	9.0 ± 0	13	9.0 ± 0	13
9	20 mg/mL Zn-C	9.3 ± 0.6	17	9.0 ± 0	13
10	Chloramphenicol	15.3 ± 0.6	92	24.7 ± 0.6	208

carboxymethyl starch/ZnO for wound dressing applications [41], but they contradict previous research suggesting that ZnO can enhance the mechanical properties of sodium alginate-based hydrogels [22, 35]. The reason for the decreased tensile strength might be due to the agglomeration of Zn Ps in the hydrogel network, [41] the interference of the ionic crosslinking process by Zn Ps, or the decreased crystallinity of the hydrogels, as shown by XRD analysis.

Antibacterial Activities of the Zn Ps and Hydrogels Containing Zn Ps

The antibacterial activities of Zn Ps were assessed against Gram-positive *S. aureus* and Gram-negative *E. coli* using the disc diffusion method at various concentrations (5, 10, and 20 mg/mL). All Zn Ps exhibited a distinct zone of inhibition (ZOI) ranging from 8.3 mm to 19.7 mm, depending on the concentrations and types of Zn Ps (Table 1; Fig. 7a). Interestingly, Zn-HA showed the highest ZOI compared to ZN-C and Zn-N, with an inhibition percentage of 146 at a concentration of 20 mg/mL for *S. aureus*. Zn-HA showed a higher ZOI against *S. aureus* than *E. coli*, which is in agreement with previous studies [42–44]. This tendency towards Gram-positive bacteria may be explained by discrepancies in cell structure, such as the presence of lipopolysaccharides in the outer membrane of Gram-negative bacteria [45], as well as differences in metabolism between Gram-positive and Gram-negative bacteria [44]. Notably, no bacterial inhibition was observed at concentrations < 2.5 mg/mL (data not shown).

The inhibitory concentration observed in this study far exceeds the reported minimum inhibitory concentration (MIC) of ZnO for these bacteria, which ranges from 25 µg/mL to 1.25 mg/mL [42, 44, 46–49]. These findings were somewhat unexpected, given prior research suggesting the potent antibacterial properties of ZnO [50–52]. We hypothesize that the enhanced antibacterial capabilities of Zn-HA may be attributed to the increased release of Zn^{2+} (7.5 mg/100 mL compared to 0.8 and 1.2 mg/100 mL) (Fig. S5a) [38, 53]. This increase could be due to the enhanced hydrogen bonding interactions between water molecules, thereby promoting Zn-HA solubility [54]. In addition, ZnO possesses a more stable crystalline structure, rendering it insoluble in water and resulting in a slower release of Zn^{2+} through a dissolution process [55]. Other possible mechanisms include the generation of ROS through Zn^{2+} dissolution [56] and mechanical damage to the bacterial membrane caused by the direct contact between Zn-HA and bacteria [57]. Additional research is required to validate this hypothesis and to understand the mechanism underlying the enhanced antibacterial efficacy of Zn-HA.

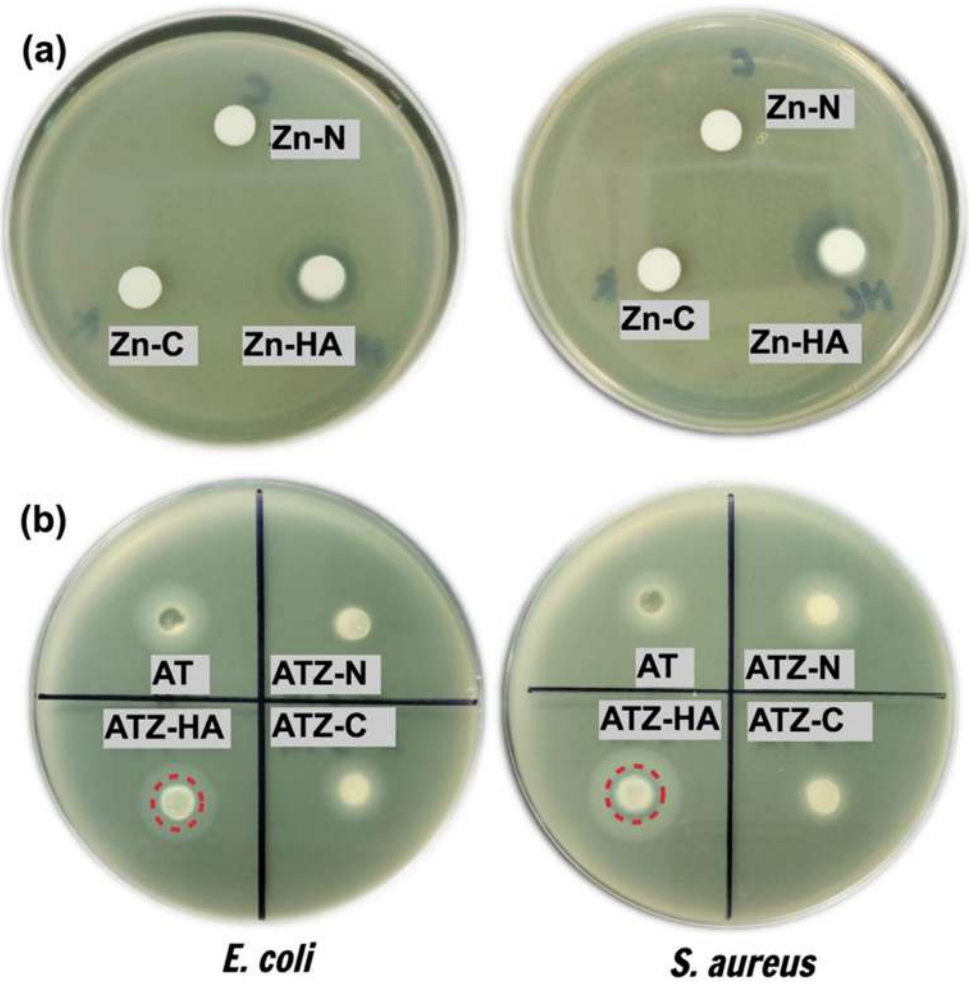

Fig. 7 Antibacterial activity of Zn Ps (**a**) and AT hydrogels embedded with Zn Ps (**b**). The red dashed circle indicates ZOI

Table 2 The results of zone of inhibition (ZOI) and inhibition percentage for AT/Zn Ps hydrogels at a concentration of 20 mg/mL

No	Samples	Type of bacteria			
		E. coli		S. aureus	
		Zone of inhibition (ZOI)			
		Diameter (mm)	% Inhibition	Diameter (mm)	% Inhibition
1	AT	8.0 ± 0.0	0	8.0 ± 0.0	0
2	ATZ-N	8.0 ± 0.0	0	8.0 ± 0.0	0
3	ATZ-HA	9.0 ± 0.0	13	9.0 ± 0.6	17
4	ATZ-C	8.0 ± 0.0	0	8.0 ± 0.0	0

The findings of our study revealed that a concentration of 20 mg/mL Zn Ps exhibited the largest inhibition zone, indicating its superior efficacy in suppressing bacterial growth. Consequently, we employed a concentration of 20 mg/mL of Zn Ps in the hydrogel system. Consistent with previous findings, the hydrogel system with Zn-HA (ATZ-HA) exhibited superior outcomes compared to the hydrogels with Zn-C (ATZ-C) and Zn-N (ATZ-N) (Fig. 7b; Table 2). Nevertheless, the bacterial inhibition was considerably lower in the hydrogel system, potentially attributable to the delayed release of Zn^{2+} ions from the hydrogel matrix (Fig. S5b). Our findings suggest that there is no need to convert Zn-HA to ZnO to impart antibacterial capabilities to the hydrogels, as the Zn-HA itself exhibits strong antibacterial properties. This simplifies the production process and reduces manufacturing costs. Thus, AT hydrogels with Zn-HA (ATZ-HA) have the potential to be utilized as antibacterial materials. A summary of the antibacterial properties of the hydrogels is shown in Table 3, including the in vitro biocompatibility, which will be discussed in the following section.

In Vitro Biocompatibility of the Hydrogels

The in vitro biocompatibility of the hydrogels was assessed using the MTS assay, which measures cell viability and proliferation in response to hydrogels. In this study, we employed an indirect assay utilizing leach-out products from hydrogels (hydrogel extracts) at a concentration of 0.1 mg/mL. Figure 8 shows the cell viability of human skin fibroblasts treated with hydrogels compared to the control. All hydrogels exhibited a decrease in cell viability, with the lowest cell viability observed in ATZ-N at 60%. However,

Table 3 Comparison of antibacterial activity, Zn^{2+} release, and in vitro biocompatibility of the hydrogels

Hydrogels	Zn Ps	Type of bacteria	% Inhibition	Zn^{2+} release (mg/100 mL)	Cell viability (%)
AT	-	*E. coli*	*NA*	-	71.8 ± 5.1
		S. aureus	*NA*		
ATZ-N	ZnO NPs	*E. coli*	*NA*	0.21 ± 0.01	60.2 ± 9.4
		S. aureus	*NA*		
ATZ-HA	Zn-HA	*E. coli*	13	0.96 ± 0.01	62.6 ± 5.8
		S. aureus	17		
ATZ-C	ZnO	*E. coli*	*NA*	0.58 ± 0.01	70.6 ± 11
		S. aureus	*NA*		

NA: no bacterial inhibition was observed

no statistically significant differences in cell viability were observed between the hydrogels. The cell viability observed in all hydrogels was above 50%, indicating that they are considered to have mild toxicity, based on the ISO 10993-5:2009(E) criteria [30]. This decrease in cell viability was possibly due to the presence of TOCN in the hydrogels, as documented in previous studies [58, 59]. In addition, the higher concentrations of Zn^{2+} used in this study also contributed to reduced cell viability [56, 60]. It is important to note that the MTS assay used in this study may not fully capture the potential cytotoxic effects of hydrogels, as it measures metabolic activity rather than the number of cells [61, 62]. In addition, certain materials, including hydrogel components, may interfere with the MTS assay, leading to false-positive or false-negative results [62, 63]. Further studies using additional assays to assess cell viability and toxicity are warranted to fully understand the impact of these hydrogels on the cells.

Conclusions

We fabricated composite alginate/TOCN (AT) hydrogels incorporating different forms of zinc particles (Zn Ps) (Zn-N, Zn-HA, and Zn-C) and compared their antibacterial effectiveness. All Zn Ps exhibited negative charges and displayed sufficient colloidal stability, with a zeta potential ranging from − 16.7 mV to -34.7 mV. The dispersion of Zn Ps within the hydrogel matrix was confirmed through EDX and XRD analysis. However, the addition of Zn Ps led to a reduction in the mechanical properties and swelling behavior of the hydrogels, as evidenced by a decrease in tensile strength, crystallinity, and swelling (%). Moreover, the antibacterial activity of Zn Ps was found to be both concentration-dependent and specific to the type of Zn Ps, with Zn-HA demonstrating the highest effectiveness against both Gram-positive *S. aureus* and Gram-negative *E. coli*. Among three types of hydrogels (ATZ-N, ATZ-C, and ATZ-HA), only ATZ-HA showed antibacterial activity against both *S. aureus* and *E. coli*, which might be due to the higher Zn^{2+} release from Zn-HA as compared to the more stable ZnO wurtzite structures of Zn-N and Zn-C, which were dispersed in ATZ-N and ATZ-C, as determined by zinc dissolution and release

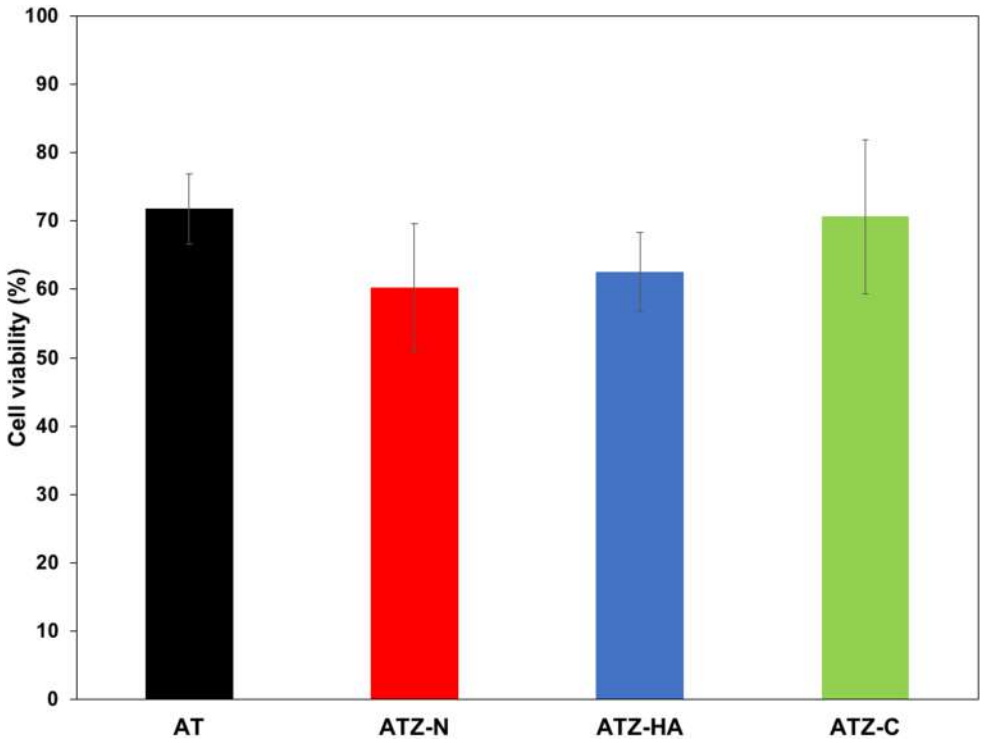

Fig. 8 Cell viability of human skin fibroblasts treated with the hydrogels after 24 h of incubation as determined by the MTS assay. Hydrogel extracts at a concentration of 0.1 mg/mL were used

studies. Given the mild toxicity and antibacterial activity of the ATZ-HA hydrogels, this research sets the foundation for further investigation into its potential applications in wound healing and infection control. Future studies should focus on elucidating the underlying mechanisms of the enhanced antibacterial activity of Zn-HA at the cellular and molecular levels and optimizing the Zn-HA formulation to maintain cell viability while maximizing antibacterial efficacy for biomedical-related applications.

Supplementary Information The online version contains supplementary material available at https://doi.org/10.1007/s10876-024-02632-x.

Acknowledgements The authors acknowledge the financial support provided by the Directorate of Talent Management BRIN for the post-doctoral scheme to M.A.R. (SK Deputi Bidang Sumber Daya Manusia IPTEK BRIN No.86/II/HK/2023). We also thank the Advanced Characterization laboratory through the E-layanan sains (ELSA) and PT. Cipta Mikro Material (CMiM) for the facilities and equipment provided for the material analysis.

Author Contributions MAR: Conceptualization, Investigation, Writing-original draft. GET: Conceptualization, Review-editing. DSK: Review-editing. NPRAK: Investigation, Review-editing. APP: Investigation, review-editing. LA: Investigation, Review-editing, WR: Review-editing. SDH: Review-editing. MI: Investigation, Review-editing. NH: Supervision, Funding acquisition, Review-editing.

Funding This research was supported by the Directorate of Talent Management BRIN (No. 86/II/HK/2023).

Data Availability No datasets were generated or analysed during the current study.

Declarations

Ethical Approval Not applicable.

Competing Interests The authors declare no competing interests.

References

1. Sartika D, Syamsu K, Warsiki E, et al (2021) Nanocrystalline Cellulose from Kapok Fiber (Ceiba pentandra) and its Reinforcement Effect on Alginate Hydrogel Bead. Starch/Staerke 73:1–12. https://doi.org/10.1002/star.202100033
2. Kumar M, Hilles AR, Ge Y, et al (2023) A review on polysaccharides mediated electrospun nanofibers for diabetic wound healing: Their current status with regulatory perspective. Int J Biol Macromol 234:. https://doi.org/10.1016/j.ijbiomac.2023.123696
3. Xie L, Wei H, Kou L, et al (2020) Antibiotic drug release behavior of poly (vinyl alcohol)/sodium alginate hydrogels. Materwiss Werksttech 51:850–855. https://doi.org/10.1002/mawe.201900163
4. Chalitangkoon J, Wongkittisin M, Monvisade P (2020) Silver loaded hydroxyethylacryl chitosan/sodium alginate hydrogel films for controlled drug release wound dressings. Int J Biol Macromol 159:194–203. https://doi.org/10.1016/j.ijbiomac.2020.05.061
5. Isogai A, Saito T, Fukuzumi H (2011) TEMPO-oxidized cellulose nanofibers. Nanoscale 3:71–85. https://doi.org/10.1039/c0nr00583e
6. Kafy A, Kim HC, Zhai L, et al (2017) Cellulose long fibers fabricated from cellulose nanofibers and its strong and tough characteristics. Sci Rep 7:1–8. https://doi.org/10.1038/s41598-017-17713-3
7. Markstedt K, Mantas A, Tournier I, et al (2015) 3D bioprinting human chondrocytes with nanocellulose-alginate bioink for cartilage tissue engineering applications. Biomacromolecules 16:1489–1496. https://doi.org/10.1021/acs.biomac.5b00188
8. Park M, Lee D, Hyun J (2015) Nanocellulose-alginate hydrogel for cell encapsulation. Carbohydr Polym 116:223–228. https://doi.org/10.1016/j.carbpol.2014.07.059
9. Aarstad O, Heggset EB, Pedersen IS, et al (2017) Mechanical properties of composite hydrogels of alginate and cellulose nanofibrils. Polymers (Basel) 9:. https://doi.org/10.3390/polym9080378
10. Li Y, Wang C, Chen T (2022) Preparation of pH-responsive cellulose nanofibril / sodium alginate based hydrogels for drug release. J Appl Polym Sci 139:e51647. https://doi.org/10.1002/app.51647
11. Putra BU, Hardiningtyas SD, Hastuti N, et al (2024) Alginate hydrogel incorporating cellulose nanofiber from solid waste agar industry for hydrophobic antibiotic delivery: Synthesis and characterization. Mater Today Commun 38:108248. https://doi.org/10.1016/j.mtcomm.2024.108248
12. Król A, Pomastowski P, Rafińska K, et al (2017) Zinc oxide nanoparticles: Synthesis, antiseptic activity and toxicity mechanism. Adv Colloid Interface Sci 249:37–52. https://doi.org/10.1016/j.cis.2017.07.033
13. Vedhanayagam M, Unni Nair B, Sreeram KJ (2018) Collagen-ZnO Scaffolds for Wound Healing Applications: Role of Dendrimer Functionalization and Nanoparticle Morphology. ACS Appl Bio Mater 1:1942–1958. https://doi.org/10.1021/acsabm.8b00491
14. Zare M, Namratha K, Ilyas S, et al (2022) Emerging Trends for ZnO Nanoparticles and Their Applications in Food Packaging. ACS Food Sci Technol. https://doi.org/10.1021/acsfoodscitech.2c00043
15. Kim I, Viswanathan K, Kasi G, et al (2022) ZnO Nanostructures in Active Antibacterial Food Packaging: Preparation Methods, Antimicrobial Mechanisms, Safety Issues, Future Prospects, and Challenges. Food Rev Int 38:537–565. https://doi.org/10.1080/87559129.2020.1737709
16. Puspasari V, Ridhova A, Hermawan A, et al (2022) ZnO-based antimicrobial coatings for biomedical applications. Bioprocess Biosyst Eng 45:1421–1445. https://doi.org/10.1007/s00449-022-02733-9
17. Happy Agarwal, Menon S, Venkat Kumar S, Rajeshkumar S (2018) Mechanistic study on antibacterial action of zinc oxide nanoparticles synthesized using green route. Chem Biol Interact 286:60–70. https://doi.org/10.1016/j.cbi.2018.03.008
18. Khalid A, Khan R, Ul-Islam M, et al (2017) Bacterial cellulose-zinc oxide nanocomposites as a novel dressing system for burn wounds. Carbohydr Polym 164:214–221. https://doi.org/10.1016/j.carbpol.2017.01.061
19. Kaptan Y, Karal-Yilmaz O, Izbudak B, et al (2023) Preparation of tetracycline hydrochloride loaded chitosan/silk fibroin/ZnO antibacterial biocomposite hydrogel sponges for wound healing application. J Polym Res 30:1–17. https://doi.org/10.1007/s10965-022-03435-2
20. Chen Y, Chen J, Chen K, Qiu H (2024) Preparation and properties of antibacterial composite hydrogels based on polyvinyl alcohol, chitosan, and nano-metal oxide. Cellulose. https://doi.org/10.1007/s10570-024-05821-z

21. Zhai X, Hu H, Hu M, et al (2024) A nano-composite hyaluronic acid-based hydrogel efficiently antibacterial and scavenges ROS for promoting infected diabetic wound healing. Carbohydr Polym 334:122064. https://doi.org/10.1016/j.carbpol.2024.122064
22. Varaprasad K, Malegowd G, Jayaramudu T, Seo J (2016) Nano zinc oxide–sodium alginate antibacterial cellulose fibres. Carbohydr Polym 135:349–355
23. Shefa AA, Taz M, Hossain M, et al (2019) Investigation of efficiency of a novel, zinc oxide loaded TEMPO-oxidized cellulose nanofiber based hemostat for topical bleeding. Int J Biol Macromol 126:786–795. https://doi.org/10.1016/j.ijbiomac.2018.12.079
24. Hastuti N, Darmayanti RF, Hardiningtyas SD, et al (2019) Nanocellulose from oil palm biomass to enhance microbial fermentation of butanol for bioenergy applications. BioResources 14:6936–6957. https://doi.org/10.15376/biores.14.3.6936-6957
25. Lee KS, Park CW, Kim JD (2017) Electrochemical properties and characterization of various ZnO structures using a precipitation method. Colloids Surfaces A Physicochem Eng Asp 512:87–92. https://doi.org/10.1016/j.colsurfa.2016.10.022
26. Alias SS, Ismail AB, Mohamad AA (2010) Effect of pH on ZnO nanoparticle properties synthesized by sol-gel centrifugation. J Alloys Compd 499:231–237. https://doi.org/10.1016/j.jallcom.2010.03.174
27. Schlur L, Carton A, Pourroy genevieve (2015) A new zinc hydroxy acetate hydrogen carbonate lamellar phase for growing large and clean ZnO nanorods arrays. Chem Comm 51:3367–3370
28. Patel DK, Dutta SD, Shin WC, et al (2021) Fabrication and characterization of 3D printable nanocellulose-based hydrogels for tissue engineering. RSC Adv 11:7466–7478. https://doi.org/10.1039/d0ra09620b
29. Sholekha S, Budiarti S, Hasan AEZ, et al (2024) Antimicrobial Potential of an Actinomycete Gordonia terrae JSN1.9-Derived Orange Pigment Extract. HAYATI J Biosci 31:161–170. https://doi.org/10.4308/hjb.31.1.161-170
30. Ningrum DR, Hanif W, Mardhian DF, Asri LATW (2023) In Vitro Biocompatibility of Hydrogel Polyvinyl Alcohol/Moringa oleifera Leaf Extract/Graphene Oxide for Wound Dressing. Polymers (Basel) 15:. https://doi.org/10.3390/polym15020468
31. Ning R, Takeuchi M, Lin JM, et al (2018) Influence of the morphology of zinc oxide nanoparticles on the properties of zinc oxide/nanocellulose composite films. React Funct Polym 131:293–298. https://doi.org/10.1016/j.reactfunctpolym.2018.08.005
32. Ba-Abbad MM, Kadhum AAH, Bakar Mohamad A, et al (2013) The effect of process parameters on the size of ZnO nanoparticles synthesized via the sol-gel technique. J Alloys Compd 550:63–70. https://doi.org/10.1016/j.jallcom.2012.09.076
33. Abd Mutalib M, Rahman MA, Othman MHD, et al (2017) Scanning Electron Microscopy (SEM) and Energy-Dispersive X-Ray (EDX) Spectroscopy. Elsevier B.V.
34. Ma H, Zhao J, Liu Y, et al (2023) Controlled delivery of aspirin from nanocellulose-sodium alginate interpenetrating network hydrogels. Ind Crops Prod 192:116081. https://doi.org/10.1016/j.indcrop.2022.116081
35. Wang T, Wang J, Wang R, et al (2019) Preparation and properties of ZnO/sodium alginate bi-layered hydrogel films as novel wound dressings. New J Chem 43:8684–8693. https://doi.org/10.1039/c9nj00402e
36. Albarqi HA, Alqahtani AA, Ullah I, et al (2022) Microwave-Assisted Physically Cross-Linked Chitosan-Sodium Alginate Hydrogel Membrane Doped with Curcumin as a Novel Wound Healing Platform. AAPS PharmSciTech 23:. https://doi.org/10.1208/s12249-022-02222-y
37. Biranje SS, Sun J, Cheng L, et al (2022) Development of cellulose nanofibril/casein-based 3D composite hemostasis scaffold for potential wound-healing application. ACS Appl Mater Interfaces 14:3792–3808. https://doi.org/10.1021/acsami.1c21039
38. Naserian F, Mesgar AS (2022) Development of antibacterial and superabsorbent wound composite sponges containing carboxymethyl cellulose/gelatin/Cu-doped ZnO nanoparticles. Colloids Surfaces B Biointerfaces 218:112729. https://doi.org/10.1016/j.colsurfb.2022.112729
39. El-Naggar ME, Gaballah S, Abdel-Maksoud G, et al (2022) Preparation of bactericidal zinc oxide nanoparticles loaded carboxymethyl cellulose/polyethylene glycol cryogel for gap filling of archaeological bones. J Mater Res Technol 20:114–127. https://doi.org/10.1016/j.jmrt.2022.07.013
40. Sun X, Liu C, Omer AM, et al (2019) pH-sensitive ZnO/carboxymethyl cellulose/chitosan bio-nanocomposite beads for colon-specific release of 5-fluorouracil. Int J Biol Macromol 128:468–479. https://doi.org/10.1016/j.ijbiomac.2019.01.140
41. Pitpisutkul V, Prachayawarakorn J (2022) Hydroxypropyl methylcellulose/carboxymethyl starch/zinc oxide porous nanocomposite films for wound dressing application. Carbohydr Polym 298:120082. https://doi.org/10.1016/j.carbpol.2022.120082
42. Abdelbaky AS, Abd El-Mageed TA, Babalghith AO, et al (2022) Green Synthesis and Characterization of ZnO Nanoparticles Using Pelargonium odoratissimum (L.) Aqueous Leaf Extract and Their Antioxidant, Antibacterial and Anti-inflammatory Activities. Antioxidants 11:. https://doi.org/10.3390/antiox11081444
43. Álvarez-Chimal R, García-Pérez VI, Álvarez-Pérez MA, Arenas-Alatorre JÁ (2021) Green synthesis of ZnO nanoparticles using a Dysphania ambrosioides extract. Structural characterization and antibacterial properties. Mater Sci Eng C 118:111540. https://doi.org/10.1016/j.msec.2020.111540
44. Ansari MA, Murali M, Prasad D, et al (2020) Cinnamomum verum bark extract mediated green synthesis of ZnO nanoparticles and their antibacterial potentiality. Biomolecules 10:1–14. https://doi.org/10.3390/biom10020336
45. Zhou G, Li Y, Xiao W, et al (2008) Synthesis, characterization, and antibacterial activities of a novel nanohydroxyapatite/zinc oxide complex. J Biomed Mater Res - Part A 85:929–937. https://doi.org/10.1002/jbm.a.31527
46. Bala N, Saha S, Chakraborty M, et al (2015) Green synthesis of zinc oxide nanoparticles using Hibiscus subdariffa leaf extract: Effect of temperature on synthesis, anti-bacterial activity and anti-diabetic activity. RSC Adv 5:4993–5003. https://doi.org/10.1039/c4ra12784f
47. Elumalai K, Velmurugan S (2015) Green synthesis, characterization and antimicrobial activities of zinc oxide nanoparticles from the leaf extract of Azadirachta indica (L.). Appl Surf Sci 345:329–336. https://doi.org/10.1016/j.apsusc.2015.03.176
48. Sasi S, Fathima Fasna PH, Bindu Sharmila TK, et al (2022) Green synthesis of ZnO nanoparticles with enhanced photocatalytic and antibacterial activity. J Alloys Compd 924:166431. https://doi.org/10.1016/j.jallcom.2022.166431
49. Chegini V, Noghabi KA, Afshari KP, et al (2022) Biological synthesis of ZnO nanoparticles using ethanolic extract of Satureja sahendica Bornm: its characterization and antimicrobial features. Biomass Convers Biorefinery 13:16037–16048. https://doi.org/10.1007/s13399-021-02187-1
50. Sharma BK, Mehta BR, Shah E V., et al (2022) Green Synthesis of Triangular ZnO Nanoparticles Using Azadirachta indica Leaf Extract and Its Shape Dependency for Significant Antimicrobial Activity: Joint Experimental and Theoretical Investigation. J Clust Sci 33:2517–2530. https://doi.org/10.1007/s10876-021-02145-x
51. Goyal V, Singh A, Singh J, et al (2022) Biosynthesized Zinc Oxide Nanoparticles as Efficient Photocatalytic and Antimicrobial Agent. J Clust Sci 33:2551–2558. https://doi.org/10.1007/s10876-021-02108-2
52. Sajid MM, Shad NA, Javed Y, et al (2022) Efficient Photocatalytic and Antimicrobial Behaviour of Zinc Oxide Nanoplates Prepared

By Hydrothermal Method. J Clust Sci 33:773–783. https://doi.org/10.1007/s10876-021-02013-8
53. Pasquet J, Chevalier Y, Pelletier J, et al (2014) The contribution of zinc ions to the antimicrobial activity of zinc oxide. Colloids Surfaces A Physicochem Eng Asp 457:263–274. https://doi.org/10.1016/j.colsurfa.2014.05.057
54. Karavas E, Ktistis G, Xenakis A, Georgarakis E (2006) Effect of hydrogen bonding interactions on the release mechanism of felodipine from nanodispersions with polyvinylpyrrolidone. Eur J Pharm Biopharm 63:103–114. https://doi.org/10.1016/j.ejpb.2006.01.016
55. Xia T, Kovochich M, Liong M, et al (2008) Comparison of the mechanism of toxicity of zinc oxide and cerium oxide nanoparticles based on dissolution and oxidative stress properties. ACS Nano 2:2121–2134. https://doi.org/10.1021/nn800511k
56. George S, Pokhrel S, Xia T, et al (2010) Use of a rapid cytotoxicity screening approach to engineer a safer zinc oxide nanoparticle through iron doping. ACS Nano 4:15–29. https://doi.org/10.1021/nn901503q
57. Sirelkhatim A, Mahmud S, Seeni A, et al (2015) Review on zinc oxide nanoparticles: Antibacterial activity and toxicity mechanism. Nano-Micro Lett 7:219–242. https://doi.org/10.1007/s40820-015-0040-x
58. de Lima Pizi Cândido A, Fregonezi NF, Carvalho AJF, et al (2020) TEMPO-Oxidized Cellulose Nanofibers In Vitro Cytogenotoxicity Studies. Bionanoscience 10:766–772. https://doi.org/10.1007/s12668-020-00763-9
59. Ventura C, Pinto F, Lourenço AF, et al (2020) On the toxicity of cellulose nanocrystals and nanofibrils in animal and cellular models. Cellulose 27:5509–5544. https://doi.org/10.1007/s10570-020-03176-9
60. Song W, Zhang J, Guo J, et al (2010) Role of the dissolved zinc ion and reactive oxygen species in cytotoxicity of ZnO nanoparticles. Toxicol Lett 199:389–397. https://doi.org/10.1016/j.toxlet.2010.10.003
61. Claus J, Brietzke A, Lehnert C, et al (2020) Swelling characteristics and biocompatibility of ionic liquid based hydrogels for biomedical applications. PLoS One 15:1–16. https://doi.org/10.1371/journal.pone.0231421
62. Mohtar N, Parumasivam T, Gazzali AM, et al (2021) Advanced Nanoparticle-Based Drug Delivery Systems and Cancer Treatment. Cancers (Basel) 1–26
63. de Oliveira DM, Menezes DB, Andrade LR, et al (2021) Silver nanoparticles obtained from Brazilian pepper extracts with synergistic anti-microbial effect: production, characterization, hydrogel formulation, cell viability, and in vitro efficacy. Pharm Dev Technol 26:539–548. https://doi.org/10.1080/10837450.2021.1898634